

1 **Spatial segregation and aging of metabolic processes underlie phenotypic heterogeneity**
2 **in mycobacteria**

3

4 **Authors:** Celena M. Gwin^{a,*}, Kuldeepkumar R. Gupta^{a,*}, Yao Lu^a, Lin Shao^a, E. Hesper Rego^{a,1}

5

6 **Affiliations**

7 ^a Department of Microbial Pathogenesis, Yale University School of Medicine, New Haven, CT

8 06519

9 * equal contribution

10

11 ¹To whom correspondence should be addressed: hesper.rego@yale.edu

12

13 Individual cells within clonal populations of mycobacteria vary in size, growth rate, and antibiotic
14 susceptibility. Heterogeneity is, in part, determined by LamA, a protein found exclusively in
15 mycobacteria. LamA localizes to sites of new cell wall synthesis where it recruits proteins
16 important for polar growth and establishing asymmetry. Here, we report that in addition to this
17 function, LamA interacts with complexes involved in oxidative phosphorylation (OXPHOS) at a
18 subcellular location distinct from cell wall synthesis. Importantly, heterogeneity depends on a
19 unique extension of the mycobacterial ATP synthase, and LamA mediates the coupling between
20 ATP production and cell growth in single cells. Strikingly, as single cells age, concentrations of
21 proteins important for oxidative phosphorylation become less abundant, and older cells rely less
22 on oxidative phosphorylation for growth. Together, our data reveal that central metabolism is
23 spatially organized within a single mycobacterium and varies within a genetically identical
24 population of mycobacteria. Designing therapeutic regimens to account for this heterogeneity may
25 help to treat mycobacterial infections faster and more completely.

26

27 Introduction

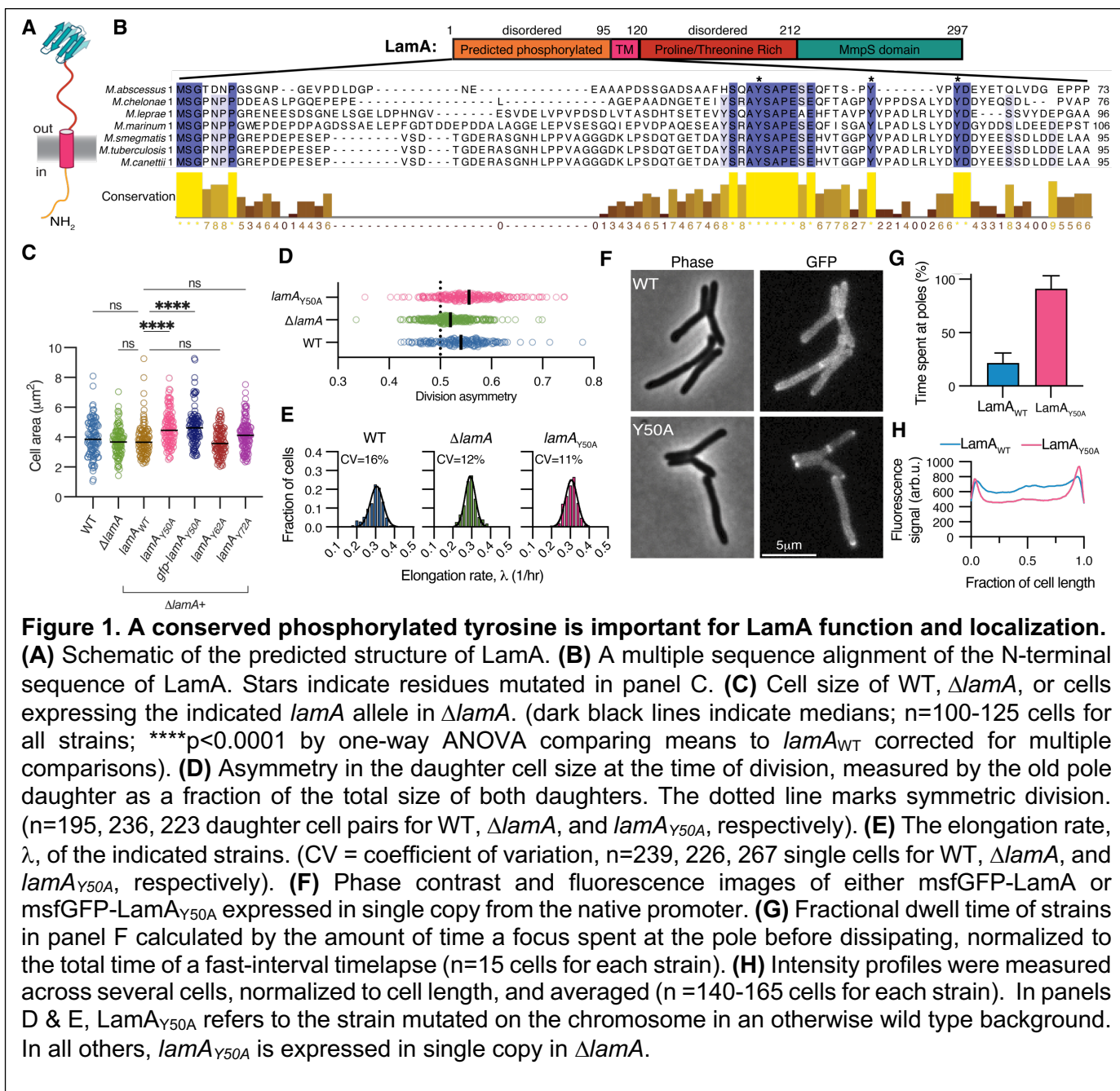
28 For a bacterial infection to linger after antibiotic treatment, only a few bacteria need to remain.
29 What is different about surviving bacteria, and how do these differences arise? Despite extensive
30 research, no single model has emerged explaining this phenomenon, and it is likely that the
31 answers to these questions will vary depending on the bacterial species. In the case of model
32 bacteria, like *Escherichia coli*, much of the focus has been on stochastic mechanisms that underlie
33 cells switching into rare drug-tolerant states (1, 2). However, stochasticity is just one way of
34 generating diversity, and other mechanisms of heterogeneity are more deterministic in nature.
35 For example, clonal populations of mycobacteria, a genus that includes the human pathogen
36 *Mycobacterium tuberculosis*, exhibit more variability than model bacterial species (3). At least
37 some of the heterogeneity is created every time a mycobacterium divides when it produces two
38 cells with different sizes, growth rates, and susceptibilities to antibiotics (4). Importantly,
39 heterogeneity is hard-coded in the genome, as deletion of a single gene unique to mycobacteria
40 – *lamA* – collapses morphological heterogeneity and leads to fast and uniform killing by several
41 antibiotics (5). LamA localizes to sites of new cell wall synthesis and recruits proteins important
42 for polar growth (6). However, many bacterial species divide asymmetrically but do not exhibit as
43 much heterogeneity as mycobacteria, suggesting that asymmetric division is only one factor
44 responsible for creating a heterogeneous population (7). Here, we sought to understand the
45 mechanism by which LamA creates heterogeneity in growth.

46

47 Results

48 A conserved tyrosine regulates the localization and function of LamA

49 The predicted structure of LamA includes two regions of high disorder separated by a single
50 transmembrane domain (**Fig. 1A**). The carboxy terminus of the protein is predicted to encode an
51 MmpS domain. Proteins with these domains are often encoded by operons that include *mmpL*
52 genes, but LamA's operon partner is a gene of unknown function. The amino terminus of LamA



53 is highly acidic, with nearly 20% of the residues in this region being either aspartic or glutamic
 54 acid. Additionally, several whole-cell proteomic studies have mapped phosphorylation events at
 55 serine, threonine, and tyrosine residues in this region (8-13). We performed a multiple sequence
 56 alignment of LamA proteins found throughout the mycobacterial genus and observed that, despite
 57 the predicted disorder of this region, several tyrosine and serine residues were highly conserved
 58 (Fig. 1B). To test the function of these residues, we created phage-integrating plasmids carrying
 59 alanine mutations at each of these sites, transformed these into $\Delta lamA$ *M. smegmatis*, and

60 imaged the resulting strains by phase contrast microscopy. To quantify the morphology of single
61 cells, we trained the U-Net machine-learning software package to detect and segment single
62 mycobacterial cells by phase contrast (14, 15). Using this approach, we found that one mutant, a
63 tyrosine mutated to an alanine at position 50, resulted in cells that were slightly larger than the
64 other mutants and wild type (**Fig. 1C**). Increased cell size was due to an increase in cell length
65 rather than width (**Fig. S1**). Importantly, tyrosine 50 is found to be phosphorylated in several
66 whole-cell proteomic studies (9-11). To confirm that this mutation is important at the native locus,
67 we used marker-less single-strained recombineering (16) to recode this tyrosine to an alanine at
68 the native locus and performed timelapse microscopy. Compared to wild type cells, a
69 subpopulation of cells expressing LamA_{Y50A} was indeed larger, driving the increased size of cells
70 across the population (**Fig. S2**). This also led to more heterogeneity in cell size at the time of
71 division; however, it did not change the asymmetry at division (**Fig. 1D, Fig S2**). Both phenotypes
72 suggested that LamA_{Y50A} functions similarly to LamA_{WT} or may be a gain-of-function mutant.

73 However, this mutant was deficient in other functions performed by LamA. Specifically,
74 LamA also affects the heterogeneity in single-cell growth rate. Biochemical fluctuations within
75 metabolic pathways result in individual cells growing at slightly different rates centered around a
76 population average (17). To compare growth rate distributions between strains, we relied on the
77 observation that single *M. smegmatis* cells grow exponentially and computed an average growth
78 rate, $\lambda = \ln(S_d/S_b)/\Delta T$, where S_d is the size of the cell at division, S_b is the size of the cell at birth,
79 and ΔT is the time between birth and division (18). Wild type *M. smegmatis* displayed 16%
80 variation in λ , in agreement with prior studies that computed λ by measuring length instead of
81 area (18, 19). In contrast, both $\Delta lamA$ and LamA_{Y50A} cells were less variable than wild type (CV_λ
82 = 12% and 11%, respectively) (**Fig. 1E**). Computing growth by other metrics resulted in the same
83 conclusion (**Fig. S3A**). Importantly, expression of LamA_{WT} from an integrative plasmid restored
84 heterogeneity in $\Delta lamA$ (**Fig. S3B**). Thus, LamA has at least two functions. One establishes

85 asymmetry in cell size at the time of division; the other is dependent on tyrosine 50 and mediates
86 heterogeneity in the growth rate of single cells.

87 To understand what was different about LamA_{Y50A}, we fused msfGFP to either the wild
88 type or mutant variant of LamA at their N-termini and expressed these from the native promoter
89 at a phage integration site in $\Delta lamA$. We had previously determined that LamA localized to the
90 septum, but were unable to visualize membrane localization, possibly due to over-expression of
91 the fusion construct (5). By expressing msfGFP fusions at native levels, we observed that, in
92 addition to localizing to the septum, msfGFP-LamA_{WT} also localizes along the sides and is
93 occasionally found at the poles (**Fig. 1E**). Timelapse imaging at 5-minute intervals confirmed that
94 msfGFP-LamA_{WT} is highly dynamic between the pole and sides of the cell, at a timescale that is
95 too fast to represent new synthesis and maturation of the fluorescence protein fusion construct
96 (**Fig. 1F-H**). We next localized msfGFP-LamA_{Y50A} and found its localization to be much less
97 dynamic, with the protein primarily localized to the poles (**Fig. 1F-H**). Interestingly, the human
98 pathogen *M. tuberculosis* divides less asymmetrically than *M. smegmatis* but, like *M. smegmatis*,
99 exhibits a wide variation in single-cell growth rates (20). As we have connected LamA to both
100 asymmetric division and growth rate heterogeneity, we wondered if the *M. tuberculosis* LamA
101 variant localized differently than *M. smegmatis* LamA. Indeed, we find the *M. tuberculosis* variant
102 of LamA expressed in *M. smegmatis* is mainly found along the side walls, with less polar
103 localization than we observe with the *M. smegmatis* variant (**Fig. S4**).

104 Taken together, these data reveal that the functions of LamA are performed at different
105 subcellular sites and that LamA dynamically localizes between these sites, possibly in a
106 phosphorylation-dependent manner. Specifically, we find that a mutant of LamA that cannot be
107 phosphorylated at a conserved residue is locked at the poles and grows more uniformly. This
108 suggests that the mechanisms used to create heterogeneity in growth are performed along the
109 sides of the bacterium. Furthermore, these data suggest that LamA functions at the pole to

110 establish asymmetric polar growth. In fact, we have recently shown that LamA is important for
111 recruiting certain proteins to the poles, which are required to establish asymmetry (6).

112

113 **LamA precipitates with proteins involved in oxidative phosphorylation, which are excluded**
114 **from the poles and septa**

115 As LamA is performing different functions at distinct subcellular sites, we hypothesized
116 that it would interact with different proteins depending on its localization. To examine this, we
117 performed a series of immunoprecipitations to find potential protein-protein interaction partners.
118 We created a strain in which the sole copy of LamA was fused to the 3X-FLAG epitope. We fixed
119 these cells with a chemical crosslinker to capture potentially transient interactions, incubated
120 lysates with α -FLAG beads, and identified co-precipitating peptides by mass spectrometry.
121 Precipitated peptides largely fell into two categories of proteins – those associated with cell
122 elongation (MmpL3, PgfA, MurA, and PknA), and those associated with cellular respiration and
123 oxidative phosphorylation (components of the electron transport chain and ATP synthase
124 complex) (**Table S1**). To verify these results, we conducted a reciprocal co-immunoprecipitation
125 with AtpG, the gamma subunit of ATP synthase, since it was highly enriched in multiple biological
126 replicates. For this, we created strains expressing both AtpG-3XFLAG and LamA-strep and found
127 that we could precipitate LamA-strep with α -FLAG beads only when AtpG-3XFLAG was present
128 (**Fig. 2A**).

129 Perhaps shedding light on these interactions, the operon containing *lamA* is arranged in
130 the middle of two operons containing many of the genes that encode proteins in the cytochrome
131 III/IV supercomplex, which performs the last step in the electron transport chain (ETC). This
132 genomic synteny is conserved across mycobacterial species (**Fig. 2B,C**). To further investigate
133 the connection between LamA and the ETC, we tracked the localization of QcrB, a subunit of the
134 III/IV supercomplex, by making an in-frame fusion to msfGFP at the chromosomal locus. We also

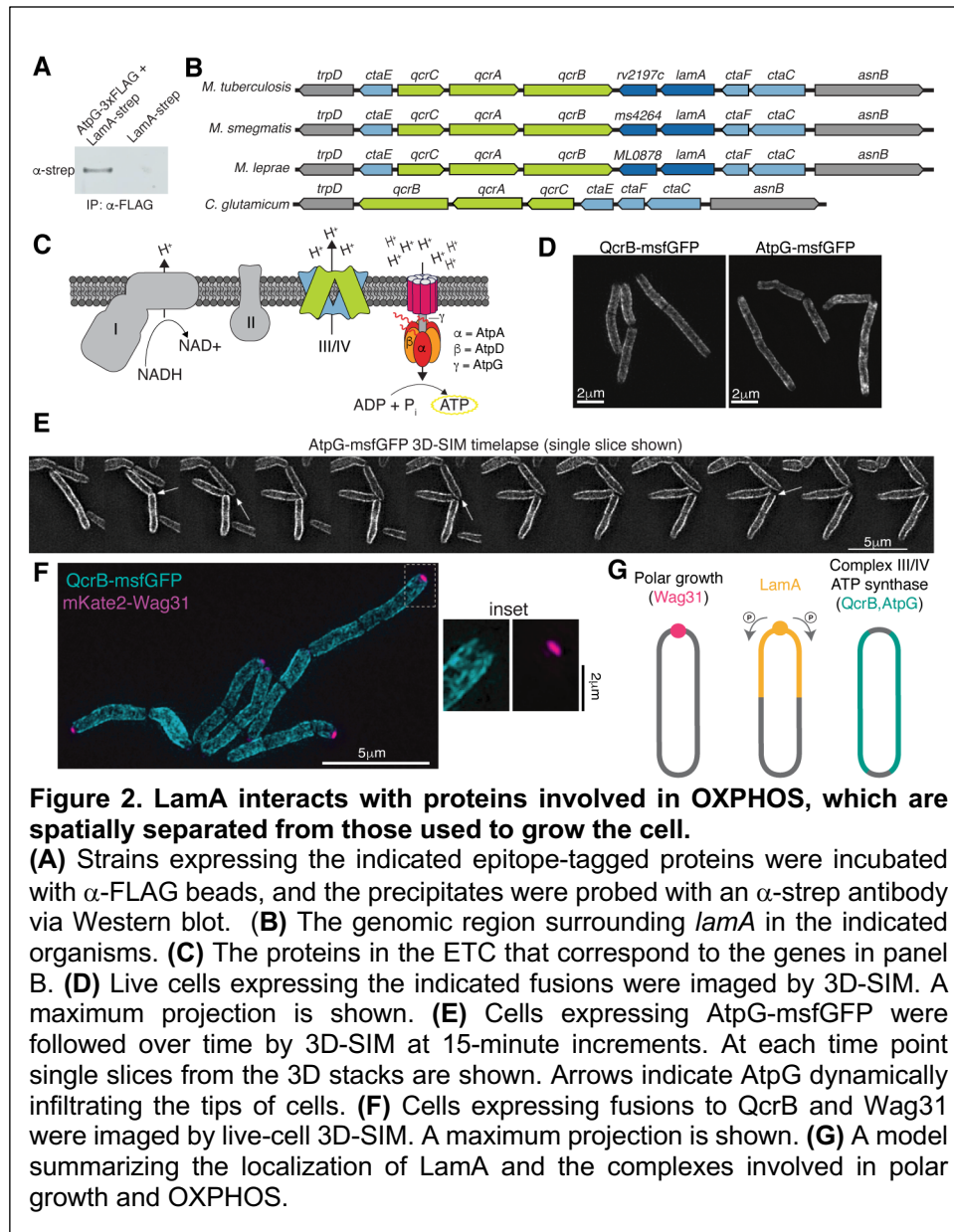


Figure 2. LamA interacts with proteins involved in OXPHOS, which are spatially separated from those used to grow the cell.

(A) Strains expressing the indicated epitope-tagged proteins were incubated with α -FLAG beads, and the precipitates were probed with an α -strep antibody via Western blot. (B) The genomic region surrounding *lamA* in the indicated organisms. (C) The proteins in the ETC that correspond to the genes in panel B. (D) Live cells expressing the indicated fusions were imaged by 3D-SIM. A maximum projection is shown. (E) Cells expressing AtpG-msfGFP were followed over time by 3D-SIM at 15-minute increments. At each time point single slices from the 3D stacks are shown. Arrows indicate AtpG dynamically infiltrating the tips of cells. (F) Cells expressing fusions to QcrB and Wag31 were imaged by live-cell 3D-SIM. A maximum projection is shown. (G) A model summarizing the localization of LamA and the complexes involved in polar growth and OXPHOS.

135 created fusions to AtpG and AtpA, the gamma and alpha subunits of the ATP synthase complex,
 136 respectively. As expected, by conventional fluorescence microscopy, the proteins were localized
 137 to the plasma membrane (Fig. S5A). To visualize the localization of these proteins more closely,
 138 we loaded cells into a microfluidic device and performed live-cell three-dimensional structured-
 139 illumination microscopy (3D-SIM), a super-resolution technique. As SIM requires collecting
 140 several images to reconstruct one super-resolved image, we focused on AtpG and QcrB fusions
 141 because these were the brightest. We collected images at single time points and observed that

142 both proteins were excluded from the tips of the cells as well as the septa of dividing cells (**Fig.**
143 **2D**). By timelapse 3D-SIM at 15-minute increments, we occasionally saw AtpG-msfGFP infiltrate
144 the tip of the cell but primarily remain localized to the sides of the cell (**Fig. 2E**). To visualize the
145 localization in the context of proteins that direct polar growth, we created a strain that encoded
146 key polar growth scaffolding protein, Wag31, fused to mKate2 in the background of cells
147 expressing QcrB-msfGFP and performed two-color live-cell 3D-SIM (**Fig. 2F,G**). We observed
148 little to no colocalization between these two proteins, showing that the complexes that perform
149 the last steps of oxidative phosphorylation are spatially distinct from those involved in growing the
150 bacterium (**Fig. 2F, Fig. S5B**). Moreover, as LamA is localized dynamically between the
151 poles/septa and sides, these data also suggest that the interaction between LamA and the
152 electron transport chain is transient and largely confined to the sides, rather than poles, of the
153 bacterium (**Fig. 2G**).

154

155 **LamA inhibits oxidative phosphorylation, and reliance on oxidative phosphorylation is**
156 **associated with uniformity.**

157 If LamA is working with the respiratory chain, we reasoned that changes to the membrane
158 potential and cellular ATP levels might reveal if it has a negative or positive regulatory role. We
159 measured membrane potential by quantifying the accumulation of a charged fluorescence
160 molecule, TMRM, by flow cytometry (21, 22). As a control, we treated cells with a known
161 protonophore, CCCP, at greater-than-MIC concentrations to depolarize the membrane and
162 observed the expected decrease in signal (**Fig. 3A**). Compared to wild type, $\Delta lamA$ was slightly
163 depolarized (**Fig. 3A**), supporting the idea that LamA is functioning with members of the electron
164 transport chain. Next, we measured ATP levels using a standard luminescence-based assay and
165 found that ATP levels were slightly higher in $\Delta lamA$ cells (**Fig. S6A**). Together, these data suggest
166 that LamA may be inhibiting the production of ATP via oxidative phosphorylation.

167 Oxidative phosphorylation is essential
 168 for mycobacteria, but mycobacteria can also
 169 produce ATP in other ways, like substrate-level
 170 phosphorylation when grown on sugars. We
 171 wondered how generalizable the connection
 172 between metabolism and heterogeneity was.
 173 Specifically, we asked if cells grown in
 174 conditions promoting the exclusive use of
 175 oxidative phosphorylation would phenocopy
 176 $\Delta lamA$. To test this, we grew cells in defined
 177 minimal media and supplied succinate as the
 178 sole carbon source. Consistent with our
 179 hypothesis, wild type *M. smegmatis* grew
 180 uniformly in minimal succinate medium, and
 181 deletion of *lamA* had no additional effect on
 182 heterogeneity (**Fig. 3B**). *M. smegmatis* cells
 183 cultured in acetate also grow uniformly (19),
 184 suggesting this phenomenon is not specific to
 185 succinate-grown cells. To understand if this
 186 was also true in slow-growing mycobacteria,
 187 we followed single *Mycobacterium bovis* BCG
 188 cells for approximately four doublings (~4
 189 days) in both our normal medium (7H9) and
 190 minimal medium supplied with succinate.
 191 Consistent with our findings in *M. smegmatis*,
 192 BCG cells cultured in 7H9 grew more

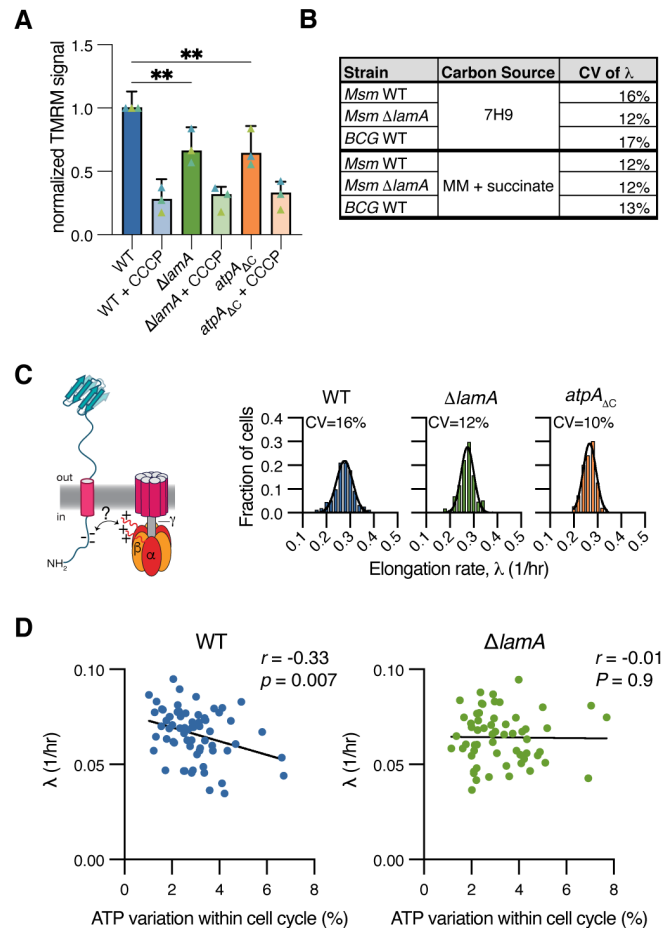


Figure 3. LamA-mediated heterogeneity is tightly linked to ATP production. (A) Accumulation of TMRM is measured by flow cytometry. As a control, cells were treated for 15 minutes with 500 μ M of CCCP. The bars represent the medians of three experiments (each with 3 biological replicates (triangles)) assayed on different days. Error bars are 95% confidence intervals. ** $p < 0.002$ by one-way ANOVA. **(B)** The indicated strains were grown in either 7H9 or minimal media (HdB for *Msm* or MMAT for *BCG*) supplied with succinate as the sole carbon source and imaged by phase contrast timelapse microscopy to compute λ for single cells. **(C)** Mycobacteria encode an unusual domain in the alpha subunit of the ATP synthase that prevents hydrolysis. We hypothesize that this positively charged extension interacts with the negatively charged cytoplasmic tail of LamA. Cells missing this extension were imaged over time to measure λ . ($n = 152$, 172, and 149 cells for WT, $\Delta lamA$, and *atpA* ΔC cells, respectively). **(D)** WT or $\Delta lamA$ cells expressing the QUEEN-2m ATP biosensor were imaged over time, and the ratio of the two QUEEN excitation wavelengths was used to obtain relative ATP levels. For each cell, the variation within a cell cycle (as measured by the standard deviation of the QUEEN-2m signal divided by its mean) was compared to the exponential growth rate ($n = 67$ and 59 complete cell cycles for WT and $\Delta lamA$, respectively; lines represent linear regressions; r is Pearson's correlation coefficient; and, p is the p -value).

193 heterogeneously than those fed only succinate ($CV_{\lambda} = 17\%$ and 13% , respectively) (**Fig. 3B**).
194 Together, these data show that cells undergoing more oxidative phosphorylation, either through
195 deletion of *lamA*, or through carbon source availability, grow more uniformly.

196

197 **An unusual extension on the ATP synthase alpha subunit mediates heterogeneity.**

198 We hypothesized that the interaction between LamA and OXPHOS proteins is important
199 for creating heterogeneity in the growth rate of single cells. The complexes that perform oxidative
200 phosphorylation in mycobacteria are comprised of highly conserved proteins, but there are
201 several unique characteristics specific to mycobacteria and related species (23). For instance, in
202 many organisms, ATP synthase can both synthesize and hydrolyze ATP depending on cellular
203 conditions. However, in some actinobacteria, including mycobacteria, the alpha subunit of ATP
204 synthase has a disordered extension (residues V519 – A548) that interacts with the gamma
205 subunit to prevent the enzyme from hydrolyzing ATP (24). The ATP synthase operon is duplicated
206 in *M. smegmatis* (25); therefore, we created a strain in which we deleted the extension in both
207 copies of *AtpA* (*atpA_{ΔC}*). Consistent with the known function of this extension to block ATP
208 hydrolysis, *atpA_{ΔC}* cells have slightly lower ATP levels (**Fig. S6B**).

209 Because the extension on *AtpA* is highly positively charged, and the N-terminal extension
210 of *LamA* is negatively charged both by amino acid residues and by multiple phosphorylated
211 residues, we hypothesized that these two proteins might be interacting electrostatically (**Fig. 3C**).
212 To that end, we reasoned that if *LamA* interacts with this extension to inhibit ATP synthase, a
213 condition we have shown is associated with more heterogeneity, then we should expect that
214 *AtpA_{ΔC}* cells would phenocopy Δ *lamA* cells with regards to both membrane potential and single-
215 cell growth heterogeneity. To test membrane potential, we used the same TMRM assay as before
216 and found that the depolarization in *atpA_{ΔC}* cells was similar in magnitude and direction as that of
217 Δ *lamA* cells (**Fig. 3A**). Next, we analyzed single-cell growth by phase contrast timelapse
218 microscopy, and consistent with our hypothesis, *atpA_{ΔC}* cells exhibit less variability in growth than

219 wild type cells (**Fig. 3C**), but not division asymmetry (**Fig. S7**). Further experiments will be needed
220 to determine if LamA and ATP synthase interact directly, a challenging directive as our data
221 suggests any interaction is likely transient. Nevertheless, we conclude that both LamA and an
222 actinobacteria-specific feature of the ATP synthase are needed to create phenotypic
223 heterogeneity within a genetically identical mycobacterial population.

224

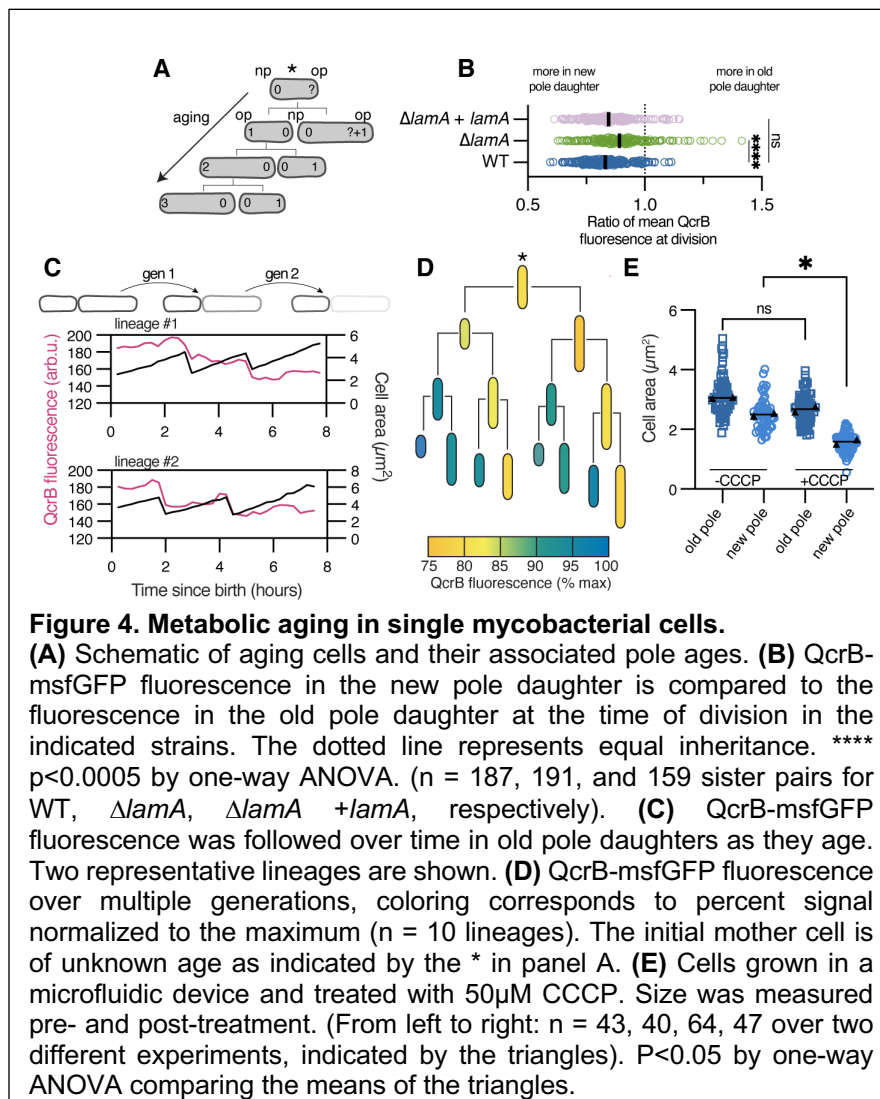
225 **LamA mediates the coupling between ATP fluctuations and growth in single cells.**

226 Cellular ATP levels are often assumed to be uniformly distributed across a population and stable
227 over the course of a cell cycle. However, fluorescent biosensors that dynamically report on ATP
228 concentrations in single bacterial cells have revealed that ATP levels vary from cell to cell and
229 fluctuate dynamically within a cell cycle (26, 27). For single cells within a clonal population, large
230 ATP fluctuations during a cell cycle are associated with slower growth (28). While the biological
231 basis for this phenomenon remains unknown, it offers a potential explanation for phenotypic
232 heterogeneity in growth rate. Since we show that LamA is connected to ATP generation through
233 oxidative phosphorylation, we hypothesized that ATP fluctuations would be altered in $\Delta lamA$ cells.
234 To assay this, we expressed a codon-optimized version of the QUEEN-2m biosensor in *M.*
235 *smegmatis* cells with and without *lamA* (26). ATP concentration within bacterial cells is linearly
236 proportional to the ratio of fluorescence excited at 405nm versus 488nm detected by the same
237 emission bandpass (26). Thus, we computed pixel-by-pixel ratios of the fluorescence values
238 collected at these wavelengths. As in *E. coli* (26), single-cell measurements revealed a negative
239 correlation between the amplitude of fluctuation of QUEEN-2m signal (*i.e.* [ATP]) and growth rate
240 in wild type *M. smegmatis* cells. On average, $\Delta lamA$ cells displayed a similar magnitude of ATP
241 fluctuation, but these fluctuations were not correlated with growth rate (**Fig. 3D**). Together, these
242 data show that LamA mediates the coupling between ATP production and growth rate across a
243 clonal population of *M. smegmatis* cells.

244

245 **Mycobacterial single-cell aging is associated with metabolic heterogeneity.**

246 After division, rod-shaped cells inherit a new pole formed from the most recent division
 247 event and an old pole that was formed during a prior division event. For mycobacteria, this means
 248 that cells inherit growing poles of various ages (**Fig. 4A**). Cells with the oldest poles are born
 249 larger but grow more slowly and with more variability (19, 29-31). As we have connected growth
 250 variability to the production of ATP, we wondered how the abundance of OXPHOS components
 251 differed as single cells aged. By timelapse microscopy, we observed that the fluorescence
 252 intensity of QcrB-msfGFP (a proxy for the cellular concentration of QcrB) was inherited unevenly
 253 at division. On average, “old pole” cells inherited a lower concentration of QcrB than their “new



254 pole” siblings. This difference was reduced in $\Delta lamA$, with a more uniform inheritance of subunits
255 between sisters (**Fig. 4A**).

256 We next asked how these differences propagated through the generations in a wild type
257 population. Thus, we identified the youngest cells in our timelapse data and followed them for at
258 least two generations. For many old pole daughters, we observed that fluorescence decreased at
259 time of division and declined steadily over multiple divisions (**Fig. 4C, 4D**). Analyzing multiple
260 lineages showed that QcrB concentration decreased in the old pole daughter cells by
261 approximately 25% after the third division (**Fig. S8A,B**). Reconstructing complete lineages
262 revealed that this phenomenon occurred to a greater or lesser degree depending on the identity
263 of the mother cell and was most pronounced in cells with the oldest mothers (**Fig. 4D**). We
264 repeated these measurements with cells expressing AtpG-msfGFP and observed similar trends
265 (**Fig. S8C,D**). Together, these data suggested that new pole progeny may be performing more
266 oxidative phosphorylation than older cells. To test this, we inhibited the proton motive force with
267 the protonophore CCCP and watched the response at the single-cell level. Consistent with our
268 hypothesis, the growth of new pole cells was affected by CCCP, while old pole cells were largely
269 unaffected (**Fig. 4E**). These results phenocopy LamA overexpression (5), further supporting the
270 notion that LamA inhibits oxidative phosphorylation. Together, these data suggest a model
271 whereby mycobacteria aging at the single-cell level is associated with less reliance on oxidative
272 phosphorylation. Consequently, in an asynchronous population of mycobacterial cells, flux
273 through central metabolism varies from cell to cell.

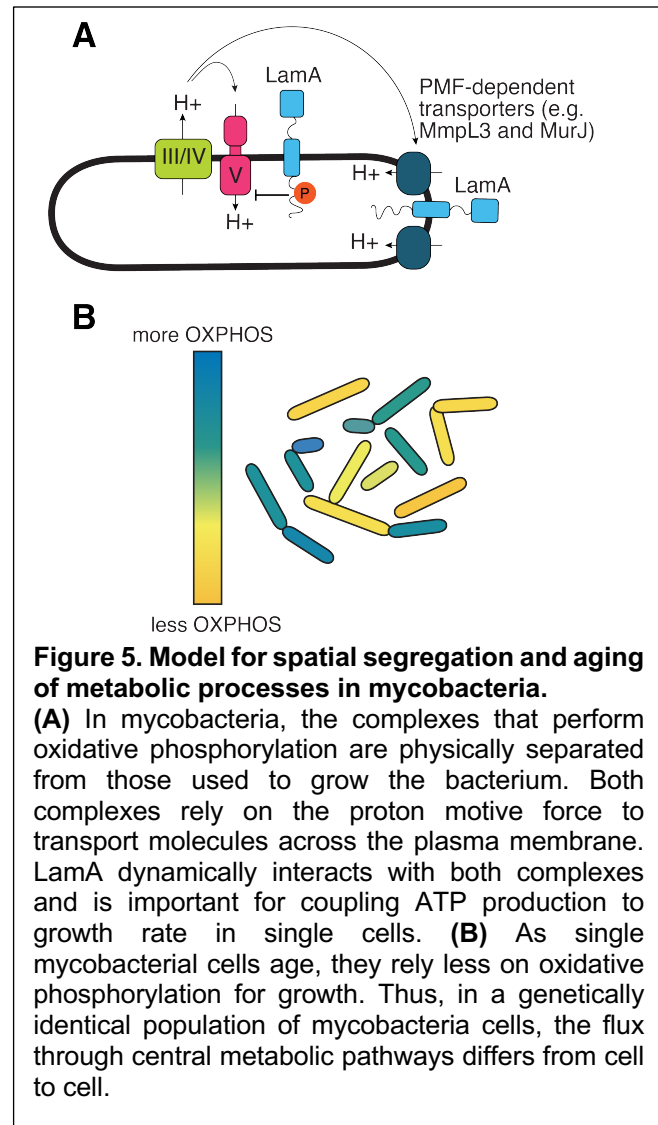
274

275 **Conclusion**

276 Despite their small size, bacteria encode diverse mechanisms to spatially structure their internal
277 biochemical processes. For example, many bacteria rely on concentration gradients along their
278 long axis to spatially organize the macromolecular machines that perform division (32-35).
279 Additionally, at division, the concentration of secondary messengers like cyclic-di-GMP, can be

280 asymmetrically distributed, an event needed
281 for the pathogenic lifecycle of *P. aeruginosa*
282 (36). Our work shows that central metabolic
283 processes like those that produce energy
284 can be subcellularly orchestrated in bacteria.
285 Further work will be needed to understand
286 the source of the connection between
287 fluctuations in ATP levels and growth of
288 single cells, which in mycobacteria is
289 mediated by LamA. We speculate that the
290 subcellular utilization of the proton motive
291 force is an important component of this
292 correlation. The proton motive force is a key
293 resource for a bacterial cell – it powers the
294 molecular machine needed to synthesize
295 ATP and is used by numerous integral
296 membrane proteins to transport various

297 substrates, including molecules that make up the cell envelope, across the plasma membrane. In
298 bacteria that grow by incorporating new envelope along their sides, complexes that use the proton
299 motive force to grow and make ATP spatially intermingle. In contrast, we show that these two
300 processes are spatially distinct in mycobacteria, with the proteins needed for oxidative
301 phosphorylation found along the sides of the bacterium and certain pumps like MmpL3 and MurJ
302 mainly localized at the poles (37-40) (Fig. 5A). Furthermore, our data suggests that LamA tra-
303 nsiently and stochastically interacts with both pathways. Supporting this observation are the
304 localizations of the likely kinase and phosphatase involved. PknA and PknB, essential kinases
305 involved in cell growth and division, are predicted to phosphorylate LamA and localize to the poles



306 (41, 42); in contrast, the only known protein phosphatase in mycobacteria, PstP, localizes along
307 the side walls and to the septum (43, 44). These data suggest that LamA could be constantly in
308 motion to generate asymmetry and heterogeneity in growth and division.

309 Mycobacteria can simultaneously catabolize different carbon sources, a feature that is
310 important for the survival of pathogenic mycobacteria which rely on a mixture of fatty acids,
311 cholesterol, and carbohydrates at different points during infection (45-47). Our data show that the
312 metabolism of mycobacteria is even more unusual than previously recognized, as a rapidly
313 growing population can diversify its metabolism at the single-cell level (**Fig. 5B**). While *M.*
314 *tuberculosis* is thought to mainly rely on cholesterol early in infection, multiple lines of evidence
315 suggest that this species uses glycolysis at later stages of infection when the bacterial burden is
316 high (48, 49). Our data suggest that this may also lead to metabolic and morphological
317 heterogeneity that may be critical for the lifecycle of the pathogen. Specifically, our model
318 suggests that inhibition of multiple metabolic subpopulations may help kill mycobacterial
319 populations faster and more completely. Indeed, simultaneous inhibition of oxidative
320 phosphorylation and glycolysis leads to rapid and complete sterilization of *M. tuberculosis* (50).
321 Thus, our data add to the growing body of evidence that understanding - and accounting for - the
322 complexity of mycobacterial physiology at the single-cell level may be the key to improving TB
323 therapy (51-55).

324

325 **References**

- 326 1. J. N. Carey *et al.*, Regulated Stochasticity in a Bacterial Signaling Network Permits
327 Tolerance to a Rapid Environmental Change. *Cell* **173**, 196-207.e114 (2018).
- 328 2. N. Q. Balaban, J. Merrin, R. Chait, L. Kowalik, S. Leibler, Bacterial Persistence as a
329 Phenotypic Switch. *Science* **305**, 1622-1625 (2004).
- 330 3. E. S. Chung, W. C. Johnson, B. B. Aldridge, Types and functions of heterogeneity in
331 mycobacteria. *Nature Reviews Microbiology* **20**, 529-541 (2022).
- 332 4. B. B. Aldridge *et al.*, Asymmetry and Aging of Mycobacterial Cells Lead to Variable
333 Growth and Antibiotic Susceptibility. *Science* **335**, 100-104 (2012).
- 334 5. E. H. Rego, R. E. Audette, E. J. Rubin, Deletion of a mycobacterial divisome factor
335 collapses single-cell phenotypic heterogeneity. *Nature* **546**, 153-157 (2017).

- 336 6. K. R. Gupta *et al.*, An essential periplasmic protein coordinates lipid trafficking and is
337 required for asymmetric polar growth in mycobacteria. *eLife* **11**, e80395 (2022).
- 338 7. M. Campos *et al.*, A constant size extension drives bacterial cell size homeostasis. *Cell*
339 **159**, 1433-1446 (2014).
- 340 8. J. Zeng *et al.*, Protein kinases PknA and PknB independently and coordinately regulate
341 essential Mycobacterium tuberculosis physiologies and antimicrobial susceptibility. *PLoS*
342 *Pathog* **16**, e1008452 (2020).
- 343 9. S. Fortuin *et al.*, Phosphoproteomics analysis of a clinical Mycobacterium tuberculosis
344 Beijing isolate: expanding the mycobacterial phosphoproteome catalog. *Front Microbiol*
345 **6**, 6 (2015).
- 346 10. K. C. Nakedi *et al.*, Identification of Novel Physiological Substrates of Mycobacterium
347 bovis BCG Protein Kinase G (PknG) by Label-free Quantitative Phosphoproteomics. *Mol*
348 *Cell Proteomics* **17**, 1365-1377 (2018).
- 349 11. S. Priscic *et al.*, Extensive phosphorylation with overlapping specificity by Mycobacterium
350 tuberculosis serine/threonine protein kinases. *Proceedings of the National Academy of*
351 *Sciences* **107**, 7521-7526 (2010).
- 352 12. R. Verma *et al.*, Quantitative Proteomic and Phosphoproteomic Analysis of H37Ra and
353 H37Rv Strains of Mycobacterium tuberculosis. *Journal of Proteome Research* **16**, 1632-
354 1645 (2017).
- 355 13. U. Kusebauch *et al.*, *Mycobacterium tuberculosis* supports protein tyrosine
356 phosphorylation. *Proceedings of the National Academy of Sciences* **111**, 9265-9270
357 (2014).
- 358 14. T. Falk *et al.*, U-Net: deep learning for cell counting, detection, and morphometry. *Nature*
359 *Methods* **16**, 67-70 (2019).
- 360 15. S. Berg *et al.*, ilastik: interactive machine learning for (bio)image analysis. *Nature*
361 *Methods* **16**, 1226-1232 (2019).
- 362 16. K. C. Murphy. (Springer US, 2021), pp. 301-321.
- 363 17. D. J. Kiviet *et al.*, Stochasticity of metabolism and growth at the single-cell level. *Nature*
364 **514**, 376-379 (2014).
- 365 18. M. M. Logsdon *et al.*, A Parallel Adder Coordinates Mycobacterial Cell-Cycle
366 Progression and Cell-Size Homeostasis in the Context of Asymmetric Growth and
367 Organization. *Current biology : CB* **27**, 3367-3374.e3367 (2017).
- 368 19. M. Priestman, P. Thomas, B. D. Robertson, V. Shahrezaei, Mycobacteria Modify Their
369 Cell Size Control under Sub-Optimal Carbon Sources. *Front Cell Dev Biol* **5**, 64 (2017).
- 370 20. E. S. Chung, P. Kar, M. Kamkaew, A. Amir, B. B. Aldridge, Mycobacterium tuberculosis
371 grows linearly at the single-cell level with larger variability than model organisms.
372 *bioRxiv*, (2023).
- 373 21. J. M. Benarroch, M. Asally, The Microbiologist's Guide to Membrane Potential
374 Dynamics. *Trends in Microbiology* **28**, 304-314 (2020).
- 375 22. J. M. Kralj, D. R. Hochbaum, A. D. Douglass, A. E. Cohen, Electrical Spiking in
376 Escherichia coli Probed with a Fluorescent Voltage-Indicating Protein. *Science* **333**, 345-
377 348 (2011).
- 378 23. H. Guo *et al.*, Structure of mycobacterial ATP synthase bound to the tuberculosis drug
379 bedaquiline. *Nature* **589**, 143-147 (2021).
- 380 24. C. F. Wong *et al.*, Structural Elements Involved in ATP Hydrolysis Inhibition and ATP
381 Synthesis of Tuberculosis and Nontuberculous Mycobacterial F-ATP Synthase Decipher
382 New Targets for Inhibitors. *Antimicrobial Agents and Chemotherapy* **66**, e01056-01022
383 (2022).
- 384 25. M. G. Montgomery, J. Petri, T. E. Spikes, J. E. Walker, Structure of the ATP synthase
385 from Mycobacterium smegmatis provides targets for treating tuberculosis. *Proceedings*
386 *of the National Academy of Sciences* **118**, e2111899118 (2021).

- 387 26. H. Yaginuma *et al.*, Diversity in ATP concentrations in a single bacterial cell population
388 revealed by quantitative single-cell imaging. *Scientific Reports* **4**, 6522 (2014).
- 389 27. S. Manuse *et al.*, Bacterial persisters are a stochastically formed subpopulation of low-
390 energy cells. *PLOS Biology* **19**, e3001194 (2021).
- 391 28. W.-H. Lin, C. Jacobs-Wagner, Connecting single-cell ATP dynamics to overflow
392 metabolism, cell growth, and the cell cycle in *Escherichia coli*. *Current Biology* **32**, 3911-
393 3924.e3914 (2022).
- 394 29. K. Ginda *et al.*, The studies of ParA and ParB dynamics reveal asymmetry of
395 chromosome segregation in mycobacteria. *Molecular Microbiology* **105**, 453-468 (2017).
- 396 30. M. M. Logsdon *et al.*, A Parallel Adder Coordinates Mycobacterial Cell-Cycle
397 Progression and Cell-Size Homeostasis in the Context of Asymmetric Growth and
398 Organization. *Current Biology* **27**, 3367-3374.e3367 (2017).
- 399 31. M. T. M. Hannebelle *et al.*, A biphasic growth model for cell pole elongation in
400 mycobacteria. *Nature Communications* **11**, (2020).
- 401 32. Y. E. Chen *et al.*, Spatial gradient of protein phosphorylation underlies replicative
402 asymmetry in a bacterium. *Proceedings of the National Academy of Sciences* **108**, 1052-
403 1057 (2011).
- 404 33. M. Thanbichler, L. Shapiro, MipZ, a Spatial Regulator Coordinating Chromosome
405 Segregation with Cell Division in *Caulobacter*. *Cell* **126**, 147-162 (2006).
- 406 34. S. Kretschmer, P. Schwillle, Pattern formation on membranes and its role in bacterial cell
407 division. *Current Opinion in Cell Biology* **38**, 52-59 (2016).
- 408 35. D. Kiekebusch, M. Thanbichler, Spatiotemporal organization of microbial cells by protein
409 concentration gradients. *Trends in Microbiology* **22**, 65-73 (2014).
- 410 36. M. Christen *et al.*, Asymmetrical Distribution of the Second Messenger c-di-GMP upon
411 Bacterial Cell Division. *Science* **328**, 1295-1297 (2010).
- 412 37. C. Carel *et al.*, Mycobacterium tuberculosis Proteins Involved in Mycolic Acid Synthesis
413 and Transport Localize Dynamically to the Old Growing Pole and Septum. *PLoS ONE* **9**,
414 e97148 (2014).
- 415 38. J. Zhu *et al.*, Spatiotemporal localization of proteins in mycobacteria. *Cell Reports* **37**,
416 110154 (2021).
- 417 39. C. L. Gee *et al.*, A Phosphorylated Pseudokinase Complex Controls Cell Wall Synthesis
418 in Mycobacteria. *Science Signaling* **5**, ra7-ra7 (2012).
- 419 40. L. Thouvenel, J. Rech, C. Guilhot, J.-Y. Bouet, C. Chalut, In vivo imaging of MmpL
420 transporters reveals distinct subcellular locations for export of mycolic acids and non-
421 essential trehalose polyphosphates in the mycobacterial outer membrane. *Scientific*
422 *Reports* **13**, (2023).
- 423 41. M. Mir *et al.*, The extracytoplasmic domain of the Mycobacterium tuberculosis Ser/Thr
424 kinase PknB binds specific muropeptides and is required for PknB localization. *PLoS*
425 *Pathog* **7**, e1002182 (2011).
- 426 42. S. N. Nagarajan *et al.*, Protein kinase A (PknA) of Mycobacterium tuberculosis is
427 independently activated and is critical for growth in vitro and survival of the pathogen in
428 the host. *J Biol Chem* **290**, 9626-9645 (2015).
- 429 43. Iswahyudi *et al.*, Mycobacterial phosphatase PstP regulates global serine threonine
430 phosphorylation and cell division. *Scientific Reports* **9**, (2019).
- 431 44. F. Shamma, E. H. Rego, C. C. Boutte, Mycobacterial serine/threonine phosphatase
432 <sc>PstP</sc> is phosphoregulated and localized to mediate control of cell wall
433 metabolism. *Molecular Microbiology* **118**, 47-60 (2022).
- 434 45. A. D. Baughn, K. Y. Rhee, Metabolomics of Central Carbon Metabolism in
435 Mycobacterium tuberculosis. *Microbiology Spectrum* **2**,
436 10.1128/microbiolspec.mgm1122-0026-2013 (2014).

- 437 46. L. P. de Carvalho *et al.*, Metabolomics of Mycobacterium tuberculosis reveals
438 compartmentalized co-catabolism of carbon substrates. *Chem Biol* **17**, 1122-1131
439 (2010).
- 440 47. Dany J. V. Beste *et al.*, ¹³C-Flux Spectral Analysis of Host-Pathogen Metabolism
441 Reveals a Mixed Diet for Intracellular Mycobacterium tuberculosis. *Chemistry & Biology*
442 **20**, 1012-1021 (2013).
- 443 48. J. Marrero, C. Trujillo, K. Y. Rhee, S. Ehrt, Glucose phosphorylation is required for
444 Mycobacterium tuberculosis persistence in mice. *PLoS Pathog* **9**, e1003116 (2013).
- 445 49. W. Y. Phong *et al.*, Characterization of phosphofructokinase activity in Mycobacterium
446 tuberculosis reveals that a functional glycolytic carbon flow is necessary to limit the
447 accumulation of toxic metabolic intermediates under hypoxia. *PLoS One* **8**, e56037
448 (2013).
- 449 50. J. S. Mackenzie *et al.*, Bedaquiline reprograms central metabolism to reveal glycolytic
450 vulnerability in Mycobacterium tuberculosis. *Nat Commun* **11**, 6092 (2020).
- 451 51. C. Toniolo, O. Rutschmann, J. D. McKinney, Do chance encounters between
452 heterogeneous cells shape the outcome of tuberculosis infections? *Current Opinion in*
453 *Microbiology* **59**, 72-78 (2021).
- 454 52. A. M. Cadena, S. M. Fortune, J. L. Flynn, Heterogeneity in tuberculosis. *Nature*
455 *reviews.Immunology*, (2017).
- 456 53. P. L. Lin *et al.*, Sterilization of granulomas is common in active and latent tuberculosis
457 despite within-host variability in bacterial killing. *Nature medicine* **20**, 75-79 (2014).
- 458 54. Q. Liu *et al.*, Tuberculosis treatment failure associated with evolution of antibiotic
459 resilience. *Science* **378**, 1111-1118 (2022).
- 460 55. M. Mistretta, N. Gangneux, G. Manina, Microfluidic dose-response platform to track the
461 dynamics of drug response in single mycobacterial cells. *Sci Rep* **12**, 19578 (2022).
- 462

463

464 **Acknowledgments.** We thank members of the Rego lab for thoughtful suggestions and
465 Dr. Andy Goodman for critical reading of the manuscript.

466 **Funding:** This work was supported by the Burroughs Wellcome Fund, the Searle
467 Foundation, the Pew Foundation, and National Institute of Health Grant R01AI148255 to
468 E.H.R. We also thank Yale Flow Cytometry for their assistance with BD Symphony
469 analyzer service. The Core is supported in part by an NCI Cancer Center Support Grant
470 # NIH P30 CA016359. The BD Symphony was funded by shared instrument grant # NIH
471 S10 OD026996. We also thank the MS & Proteomics Resource at Yale University for
472 providing the necessary mass spectrometers and the accompanying biotechnology tools
473 funded in part by the Yale School of Medicine and by the Office of The Director, National
474 Institutes of Health (S10OD02365101A1, S10OD019967, and S10OD018034). The
475 funders had no role in study design, data collection and analysis, decision to publish, or
476 preparation of the manuscript.

477 **Author contributions:** Conceptualization: C.M.G., K.R.G, and E.H.R. Investigation:
478 C.M.G., K.R.G, and E.H.R. Resources. C.M.G., K.R.G, Y.L., L.S., and E.H.R. Software:
479 L.S. Supervision: E.H.R. Funding acquisition: E.H.R. Writing - original draft: C.M.G.,
480 K.R.G, and E.H.R. Writing – review and editing: C.M.G., K.R.G, Y.L., L.S., and E.H.R

481 **Competing interests:** The authors declare no competing interests.

482 **Data and materials availability:** Strains developed during the study will be made
483 available from E.H.R.

484

485

486